Mar Geophys Res (2010) 31:133–147
DOI 10.1007/s11001-010-9097-6

ORIGINAL RESEARCH PAPER

Gas seepage, pockmarks and mud volcanoes in the near shore of SW Taiwan

Song-Chuen Chen · Shu-Kun Hsu · Ching-Hui Tsai · Chia-Yen Ku · Yi-Ching Yeh · Yunshuen Wang

Received: 2 February 2010 / Accepted: 15 August 2010 / Published online: 7 September 2010

Abstract In order to understand gas hydrate related seafloor features in the near shore area off SW Taiwan, a deep-towed sidescan sonar and sub-bottom profiler survey was conducted in 2007. Three profiles of high-resolution sub-bottom profiler reveal the existence of five gas seeps (G96, GS1, GS2, GS3 and GS4) and one pockmark (PM) in the study area. Gas seeps and pockmark PM are shown in lines A and C, while no gas venting feature is observed along line B. This is the first time that a gas-hydrate related pockmark structure has been imaged off SW Taiwan. The relatively high backscatter intensity in our sidescan sonar images indicates the existence of authigenic carbonates or chemosynthetic communities on the seafloor. More than 2,000 seafloor photos obtained by a deep-towed camera (TowCam) system confirm the relatively high backscatter intensity of sidescan sonar images related to bacteria mats and authigenic carbonates formation at gas seep G96 and pockmark PM areas. Water column gas flares are observed in sidescan sonar images along lines A and C. Likewise, EK500 echo sounder images display the gas plumes above gas seep G96, pockmark PM and gas seep GS1; the gas plumes heights reach about 150, 100 and 20 m from seafloor, respectively. Based on multichannel seismic reflection (MCS) profiles, an anticline structure trending NNE-SSW is found beneath gas seep G96, pockmark PM and gas seep GS2. It implies that the gas venting features are related to the anticline structure. A thermal fluid may migrate from the anticline structure to the ridge crest, then rises up to the seafloor along faults or fissures. The seafloor characteristics indicate that the gas seep G96 area may be in a transitional stage from the first to second stage of a gas seep self-sealing process, while the pockmark PM area is from the second to final stage. In the pockmark PM area, gas venting is observed at eastern flank but not at the bottom while authigenic carbonates are present underneath the pockmark. It implies that the fluid migration pathways could have been clogged by carbonates at the bottom and the current pathway has shifted to the eastern flank of the pockmark during the gas seep self-sealing process.

Keywords Sidescan sonar · Sub-bottom profiler · Backscatter intensity · Pockmark · Gas seep · Gas flare · Southwest Taiwan

S.-C. Chen · S.-K. Hsu · C.-H. Tsai · C.-Y. Ku · Y.-C. Yeh
Institute of Geophysics, National Central University, Chung-Li 32001, Taiwan

S.-C. Chen (✉) · Y. Wang
Central Geological Survey, Ministry of Economic Affairs, Taipei 23568, Taiwan
e-mail: songlin@moeacgs.gov.tw

Introduction

Gas seeps and mud volcanoes are generally found in permafrost and continental margins. Milkov (2000) suggested that the formation of submarine gas seeps and mud volcanoes in passive and active continental margins are due to the high sediment accumulation rate and the lateral tectonic compression. Dimitrov (2002) claimed at least one common characteristic of an overpressured source layer in the sedimentary pile. The rapid sedimentation is believed to be the main reason for overpressure in sedimentary layers (Milkov 2000; Talukder et al. 2007). Brown (1990) suggested that mud diapirs are driven by buoyancy forces due to the bulk density contrast between an overpressured muddy mass and an overburden of greater density. The additional factor of gas-charged sediments is regarded as an important factor in the diapir formation (Hovland and

Curzi 1989). However, the mechanism for mud diapirism and volcanism is not only due to the existence of overpressure layers, buoyancy forces or gas-charged sediments but also due to other factors such as tectonic faults for fluid migration pathways (Talukder et al. 2007).

In accretionary settings, mud volcanism plays an important role in the flux of fluid, solid and gas into the ocean (Deyhle and Kopf 2001). The common presence of methane in mud volcanoes provides a driving force for hydrogeologic and intrusive systems because of voluminous quantities of fluid, decreasing mud densities and increasing buoyancy forces in diapirs and entraining sediments as gas bubbles rise (Brown 1990). Therefore, methane is considered as an important role in the mechanism of mud diapirism and volcanism (Brown 1990; Hovland and Curzi 1989).

Gas seeps and mud volcanoes have been widely studied because they are generally accompanied by methane-rich fluid discharge. They are the most important pathway for methane emission from deep marine sediments into atmosphere (Dimitrov 2002, 2003). Several studies indicated the occurrence of gas seeps and mud volcanoes are closely related to the formation of gas hydrate. Therefore, the study related to the gas hydrate formation draws attention of economical interest as an energy resource. Hydrate Ridge lies within the gas hydrate stability field offshore central Oregon; several mud volcanoes and pockmark fields have documented (Johnson et al. 2003). The distribution of pockmark field is coincident with the termination of the BSR at nearly the same depth (Johnson et al. 2003). This suggests the pockmark fields may represent the gas hydrate stability limit (Johnson et al. 2003). The Dnepr paleo-delta in the NW Black Sea; almost 3,000 active methane seeps were detected (Naudts et al. 2006, 2008). The depth limit for the majority of the detected seeps corresponds more or less to the gas hydrate stability limit (Naudts et al. 2006, 2008). Numerous fluid escape features (seeps and pockmarks) found at the Storegga Slide area off Norwegian are related to the dissociation of gas hydrate (Bünz et al. 2003; Bünz and Mienert 2004; Mienert et al. 2005). Similar cases exist at Black Sea region (Klaucke et al. 2006; Krastel et al. 2003), Congo Fan area, SW Africa (Sahling et al. 2008), Mediterranean region (Iacono et al. 2008) and Nicaragua Pacific margin area (Talukder et al. 2007). It indicates that the occurrence of gas seeps and mud volcanoes is closely associated with the presence of gas hydrate.

High backscatter intensity in sidescan sonar data is generally caused by the strong acoustic impedance or roughness contrast between the seafloor surface and surrounding area (Blondel and Murton 1997). Authigenic carbonates, chemosynthetic communities or gas hydrate could cause seafloor roughness and acoustic impedance contrast in cold seep area, and thus increase acoustic backscatter intensity (Orange et al. 2002; Johnson et al. 2003; Holland et al. 2006; Talukder et al. 2007; Naudts et al. 2008). Direct seafloor photos can confirm the source for high backscatter intensity in sidescan sonar image.

Bottom simulating reflectors (BSRs) in the seismic profiles are widely observed in the offshore area of southwest Taiwan, which implies the presence of enormous amounts of gas hydrate beneath the seafloor (Liu et al. 2006). Analyses of cored sediments reveal high methane concentration (Chuang et al. 2006), shallow sulfate/methane interface (SMI) (Chuang et al. 2006; Lin et al. 2006) and common occurrence of authigenic pyrite (Jiang et al. 2006) at many sites. Anaerobic methane oxidation (AMO) is indicated by sulfate and methane depletion, hydrogen sulfide formation and an increase of alkalinity in the sediments (Chuang et al. 2006). The deep-towed camera images demonstrate fluids/gases venting structures, chemosynthetic communities of bacteria mats and clams, and widespread authigenic carbonates on the seafloor (Lin et al. 2006; Wang et al. 2007). These features indicate an active fluids/gases venting in the study area.

Mud volcanoes have been found in southern Taiwan (Yang et al. 2004). Submarine mud volcanoes, gas seeps and mud diapirs have also been reported in the offshore area of southwest Taiwan (Sun and Liu 1993; Chuang 2006a; Chiu et al. 2006; Lin et al. 2009). The submarine gas venting source could be due to the dissociation of gas hydrate and/or a deep gas reservoir (Chuang et al. 2006; Yang et al. 2006). In order to better understand the nature of gas hydrate accumulation off southwest Taiwan, in addition to MCS, a high-resolution deep-towed sidescan sonar survey was carried out in the near shore area off SW Taiwan between Kaoping and Fangliao canyons. The high resolution data allows us to identify gas venting features such as gas seeps and pockmarks. In this paper, we present the results of the deep-towed sidescan sonar survey, multichannel seismic reflection (MCS) data, EK500 sonar data and seafloor photos, which allows us better understand the relationship of gas venting features, seafloor characteristics and geological structure off SW Taiwan.

Geological background

Our study area is located off SW Taiwan, at the junction area between the Chinese continental margin in the west and the accretionary wedge of southern Taiwan in the east (Reed et al. 1992; Liu et al. 1997, 2004). A deformation front extends northward from the northern end of the Manila Trench to the Tainan area onshore Taiwan and bisects our study area (Liu et al. 2004). The accretionary wedge can be further divided into the upper and lower slope domains (Fig. 1) (Reed et al. 1992; Liu et al. 1997,

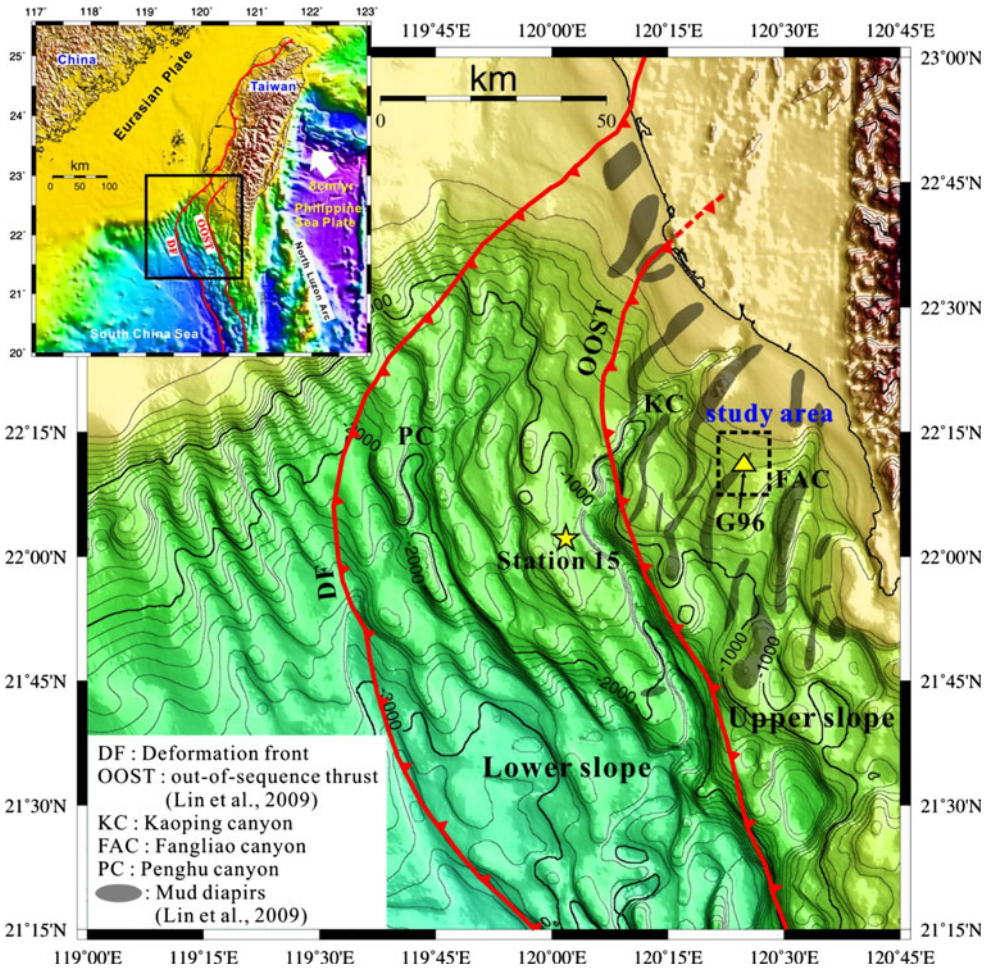

Fig. 1 Tectonic features and bathymetry off southwest Taiwan. *Inset* shows the regional topography and tectonic features. The deformation front (DF) separates the passive South China Sea (SCS) continental margin in the west and active accretionary wedge in the east. The out-of-sequence thrust (OOST) separates the *lower slope* and *upper slope* of the accretionary wedge. Mud diapirs are indicated by *gray* polygons. The station 15 and gas seep G96 are sites of thermogenic gas origin. *Dashed box* shows the location of the study area located at *upper slope* area between the Kaoping and Fangliao canyons

2006; Lin et al. 2008, 2009). The lower slope domain is characterized by a series of anticlinal ridges related to active thrusting and folding. In contrast, the upper slope domain is characterized by smooth seafloor topography and chaos of internal seismic reflection, probably due to deeply dipping beds and intense deformation (Liu et al. 2006; Lin et al. 2008, 2009). Thus, the lower slope domain is currently active in terms of thrusting and folding. However, gas venting, mud volcanoes and mud diapir structures are active in the upper slope domain (Sun and Liu 1993; Chiu et al. 2006; Chiu and Liu 2008; Chuang 2006a).

Method and data

Three deep-towed sidescan survey tracks lines A, B and C (Fig. 2) of a total length of about 22 km were collected onboard R/V Ocean Research I (ORI) in November 2007 (Fig. 2). The towing speed during the survey was between 2.0–3.0 knots and the towfish was kept at 30–50 m above the seafloor. The sidescan sonar is of a dual frequency 120 and 410 kHz. The 120 and 410 kHz modes provide across-track resolutions of 6.25 and 1.9 cm, respectively. The chirp sub-bottom profiler operates at 1–6 kHz, giving a maximum vertical resolution of 15–25 cm. The position of the towfish was calculated by a layback using the ship position, towfish height above the seafloor and cable length. This layback method gives good results except of some sections of rapid tow speed changes in view of keeping the towfish in safe condition.

Three multichannel seismic reflection (MCS) profiles (MCS896-SLC-1, 3 and 5) of 60 channels were collected by using a high resolution multichannel seismic data acquisition system onboard R/V ORI. The group interval is 12.5 m and the seismic streamer is 750 m long. The shot interval is 10 s, giving a nominal shot interval of 25 m. The air gun source is a 3-airgun array with total volume of 475 c.i. Three MCS profiles of a total length of about 32 km were collected onboard R/V ORI in April 2009 (Fig. 2). The MCS data were processed by using PROMAX interactive seismic data processing system. Along track EK500 sonar data were also collected while MCS data were collected.

Seafloor photos have been taken by a deep-towed camera (TowCam) system developed by Woods Hole Oceanographic Institution (WHOI), USA. The TowCam

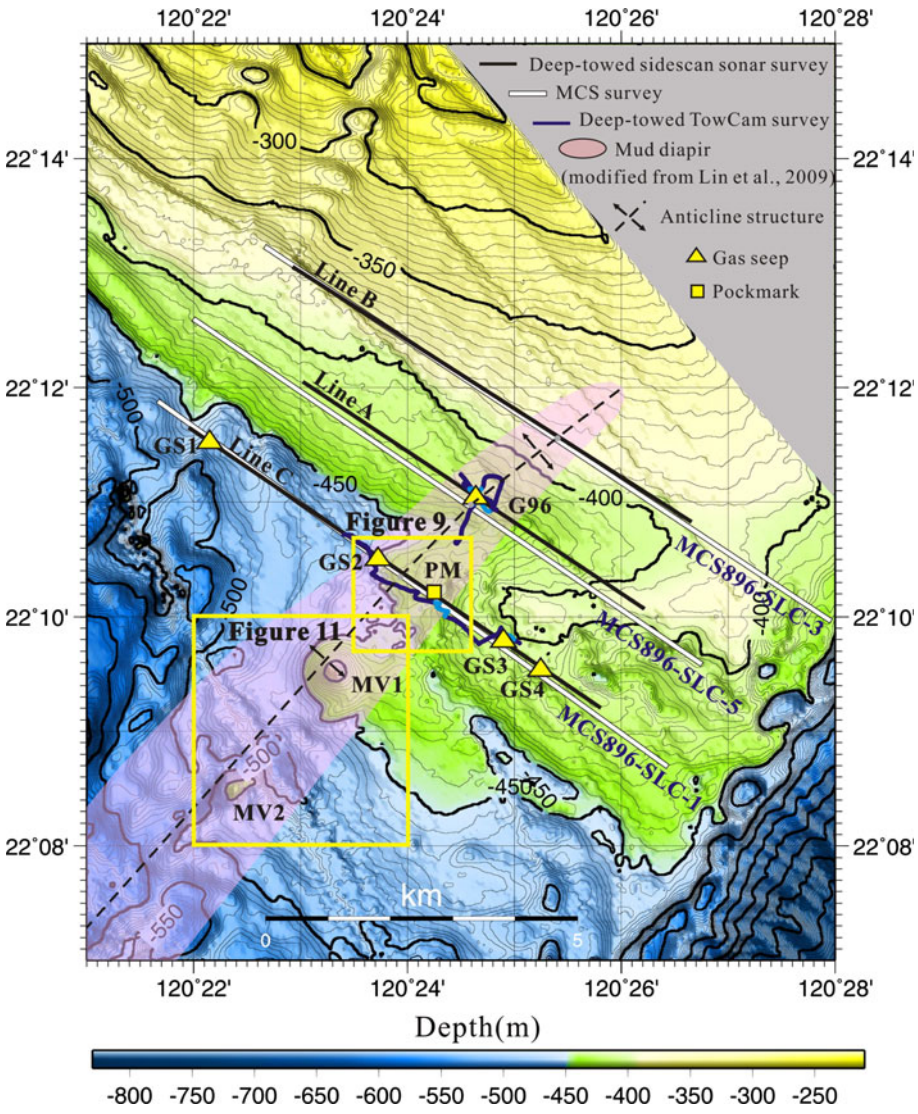

Fig. 2 Multibeam bathymetry and related structures in the study area. One pockmark (PM) and five gas seeps (G96, GS1, GS2, GS3 and GS4) are identified by deep-towed sidescan sonar data; two mud volcanoes (MV1 and MV2) are recognized based on multibeam bathymetry. The location of the study area is shown in Fig. 1

system was towed at an averaged ship speed of 0.5 knots, the digital camera was set up to take photographs at 10 s intervals and kept 2–5 m above the seafloor giving high resolution images of 338–586 pixels/m. Two TowCam survey cruises at the gas seep G96 and pockmark PM areas were conducted onboard R/V ORI in 2006 and 2008, respectively (Fig. 2). In total, more than 2,000 seafloor photos were taken during the two cruises.

Results

We have identified five gas seeps (G96, GS1, GS2, GS3 and GS4) and one pockmark (PM) along lines A and C of two deep-towed sidescan sonar survey data (Figs. 4, 5, 6, 7 and 10). In contrast, no gas venting feature is found along line B (Fig. 3). To understand the fluid migration process, a multichannel seismic reflection (MCS) survey was conducted along the same tracks of deep-towed sidescan sonar profiles. As a result, a deep anticline structure beneath the seafloor venting features is identified from the MCS profiles. Besides, two mud volcanoes (MV1 and MV2) in the south of the study area are suggested by the multibeam bathymetric data (Figs. 2 and 11).

Anticline structure

Recognized from the MCS profiles, the anticline is NNE-SSW trending and across the center of the study area (Figs. 2, 3, 4, 5 and 12). The anticline structure appears clearly in line C and line A; but, it becomes unclear towards NNE direction. It suggests that the anticline structure diminishes landward and does not extend onshore (Chuang 2006a; Sun and Liu 1993).

The gas seeps G96 and GS2 and pockmark PM are located above the anticline ridge (Figs. 4 and 5). Some fractures

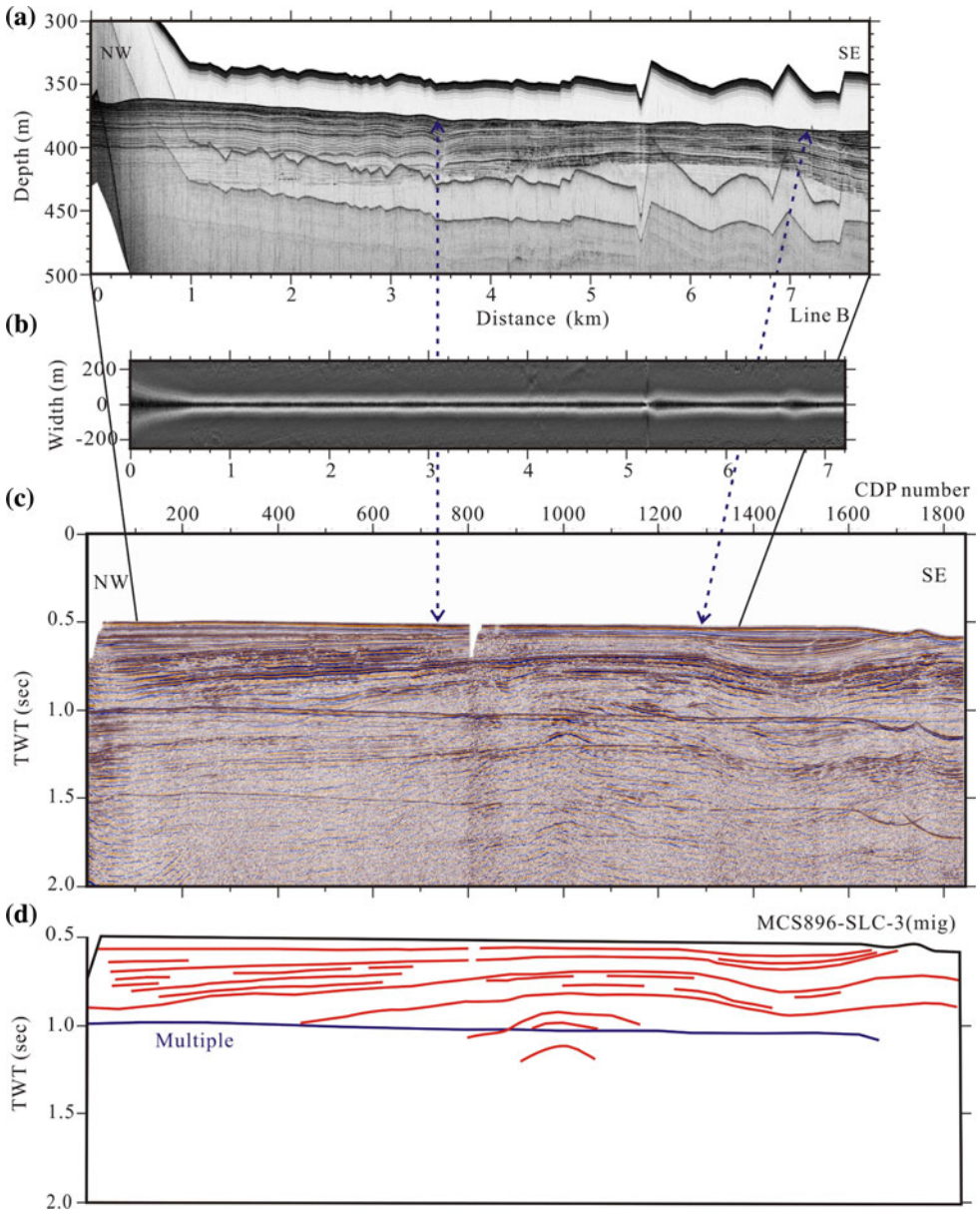

Fig. 3 **a** Sub-bottom profiler image, **b** sidescan sonar image, **c** seismic reflection profile and **d** the interpreted seismic profile of *line B*. *Note* that these is no gas venting feature. See the profile location in Fig. 2

through anticline structure may have provided conduits for fluid migration upward to seafloor and caused venting features. The multiples of the seafloor in the MCS profiles somehow disturb deep structures interpretation. However, one mud diapir structure below the anticline was mentioned by Chuang (2006a), Sun and Liu (1993) and Lin et al. (2009).

Gas seeps

Five gas seeps (G96, GS1, GS2, GS3 and GS4) have been identified in line A and line C of the sub-bottom profiler (Figs. 4, 5, 6, 7 and 10). The gas seep G96, about 310 m wide and 5 m deep at the central part, is located in line A of the sub-bottom profiler (Figs. 4, 6 and 10; Table 1). The acoustic wiped-out zone at the bottom of the gas seep indicates a gas-bearing conduit to seafloor. The sidescan sonar images also reveal a rough seafloor and relatively strong backscatter intensity (Figs. 6 and 10a). It implies the existence of authigenic carbonates or chemosynthetic communities on the seafloor (e.g. Talukder et al. 2007; Naudts et al. 2008). Our seafloor photos obtained by a deep-towed camera (TowCam) system have confirmed the bacteria mats coverage and gas venting on the rough seafloor at the gas seep G96 area (Fig. 8). The MCS profiles show the anticline structure at ~0.2 s two-ways-travel

Fig. 4 **a** EK500 sonar image, **b** sub-bottom profiler image, **c** seismic reflection profile and **d** the interpreted seismic profile of *line A*. See the profile location in Fig. 2 ▶

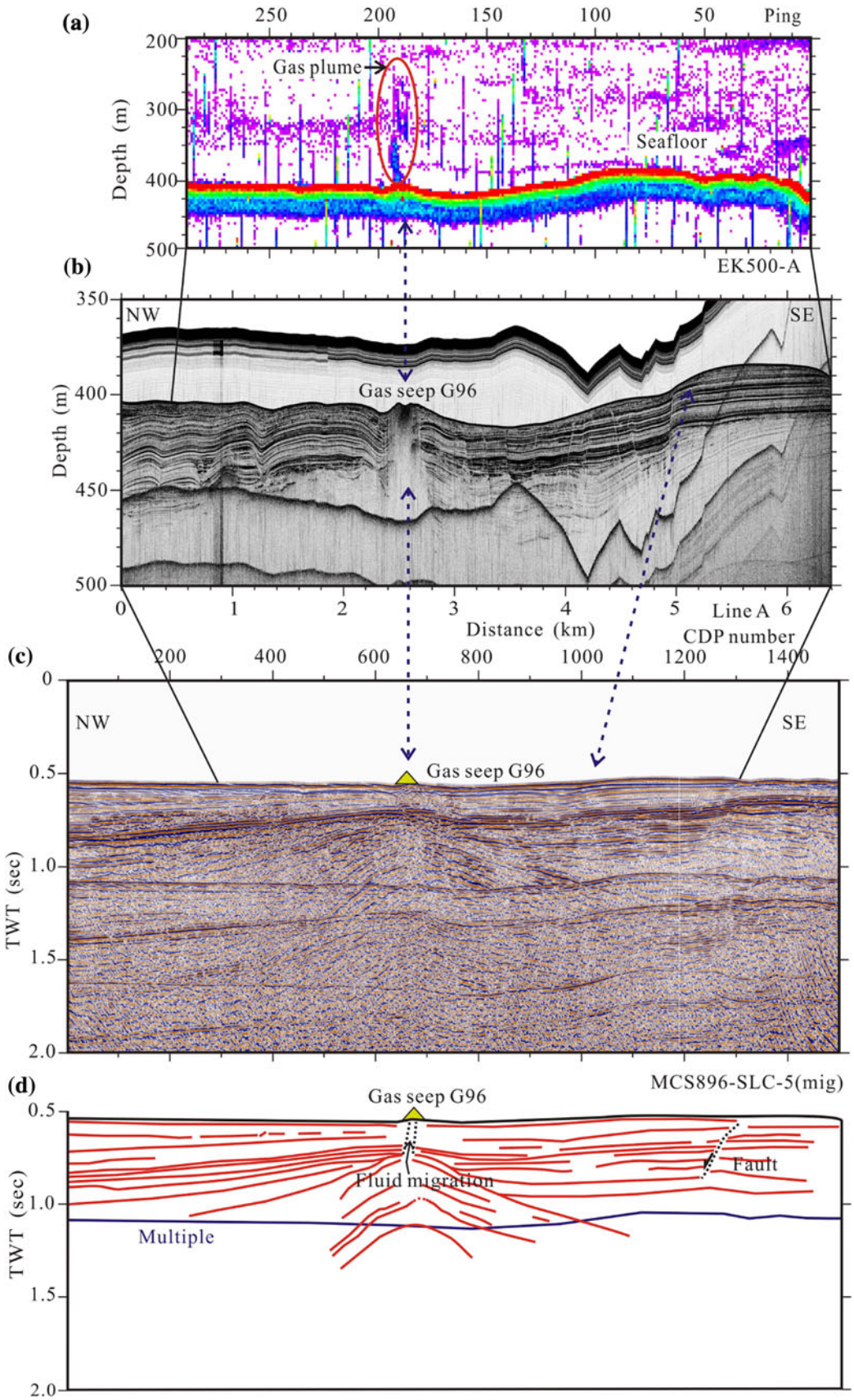
(a)
250
200
150
100
50
Ping
200
300
400
500
Depth (m)
Gas plume
Seafloor
EK500-A
(b)
350
400
450
500
Depth (m)
NW
SE
Gas seep G96
0
1
2
3
4
5
6
Distance (km)
Line A
CDP number
200
400
600
800
1000
1200
1400
(c)
0
0.5
1.0
1.5
2.0
TWT (sec)
NW
SE
Gas seep G96
MCS896-SLC-5(mig)
(d)
0.5
1.0
1.5
2.0
TWT (sec)
Gas seep G96
Fluid migration
Fault
Multiple

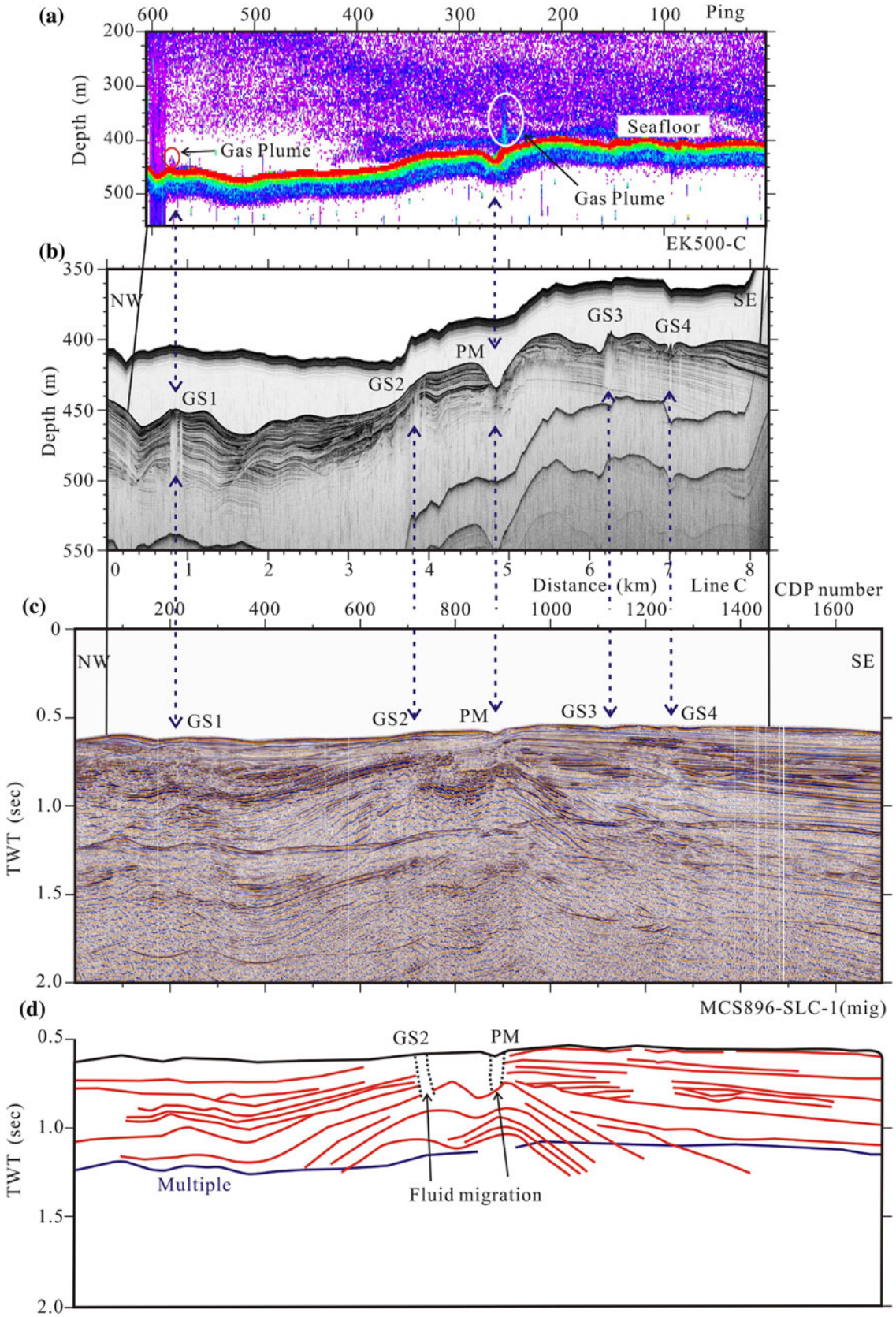

Fig. 5 **a** EK500 sonar image, **b** sub-bottom profiler image, **c** seismic reflection profile and **d** the interpreted seismic profile of *line C*. See the profile location in Fig. 2

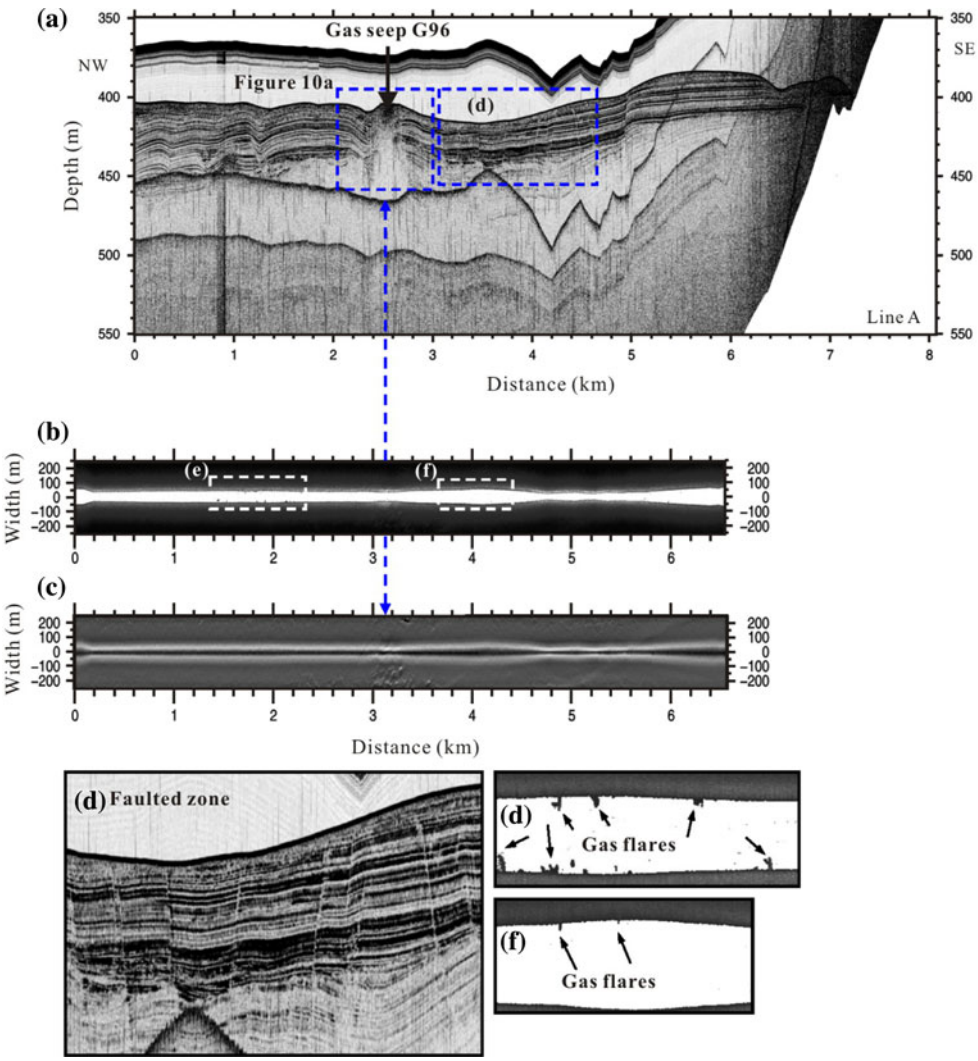

Fig. 6 Sub-bottom profiler and sidescan sonar images of *line A*. **a** *Sub-bottom* profiler image. *Note* the gas seep G96 is identified. The enlarged image of the gas seep G96 is shown in Fig. 10a. **b** Sidescan sonar image without *bottom* lock. **c** Sidescan sonar image with *bottom* lock. High backscatter intensity (*light tones*) and high rough seafloor exist at the gas seep G96 area. **d** Faulted zone in shallow sedimentary layers. **e** and **f** indicate probable gas flares. See the profile location in Fig. 2

time below the gas seep G96 (Fig. 4). Based on the EK500 sonar image, a gas plume of about 150 m high in sea water is observed above the gas seep G96 (Fig. 4). High methane anomalous in pore space, and very shallow sulfate/methane interface (<3 m) in pore water of the cored sediments were observed at site G96 (Chuang et al. 2006). The gas source is regarded as a mixture of biogenic and thermogenic gas based on the $\delta^{13}C$ composition of methane gas (Chuang 2006b). In addition, the high calculated methane flux of these sediments indicates that they were collected from actively methane-enriched vents (Chuang 2006b).

Hence, the occurrence of the gas seep G96 could be explained by the upward migration of the fluid through the anticlinal fractures at depth. The high methane flux is associated with the growth of chemosynthetic communities and authigenic carbonates precipitated due to the process of AMO on the subsurface of seafloor (Tréhu et al. 2003).

The seafloor of the gas seeps (GS1, GS2, GS3 and GS4) could be covered by authigenic carbonates or bacteria mats because relatively medium to high backscatter intensity and rough seafloor characters are displayed in the sidescan sonar images (Figs. 7 and 10). Located at 1 km west of the pockmark PM (Figs. 5 and 7), the GS2 has a width of 175 m (Fig. 10c; Table 1). The GS2 is a gas emission structure and the fluid rises upwards from the anticline ridge to seafloor through fractures as that of the pockmark PM area (see below) (Fig. 5). The 190-m wide GS1 (Fig. 10b; Table 1) is located at 3 km west of the GS2 (Figs. 5 and 7). Because the location is near the northwestern limb of the anticline (Figs. 2, 5 and 12), we infer that the source of the fluid is same as that of the gas seep GS2 and pockmark PM areas. Moreover, a 20-m high gas plume in sea water in the gas seep GS1 is found in the EK500 sonar image suggests that gas venting is active too (Fig. 5).

Two gas seeps GS3 and GS4 are located in the east of the pockmark PM (Figs. 5 and 7). The surface of the gas

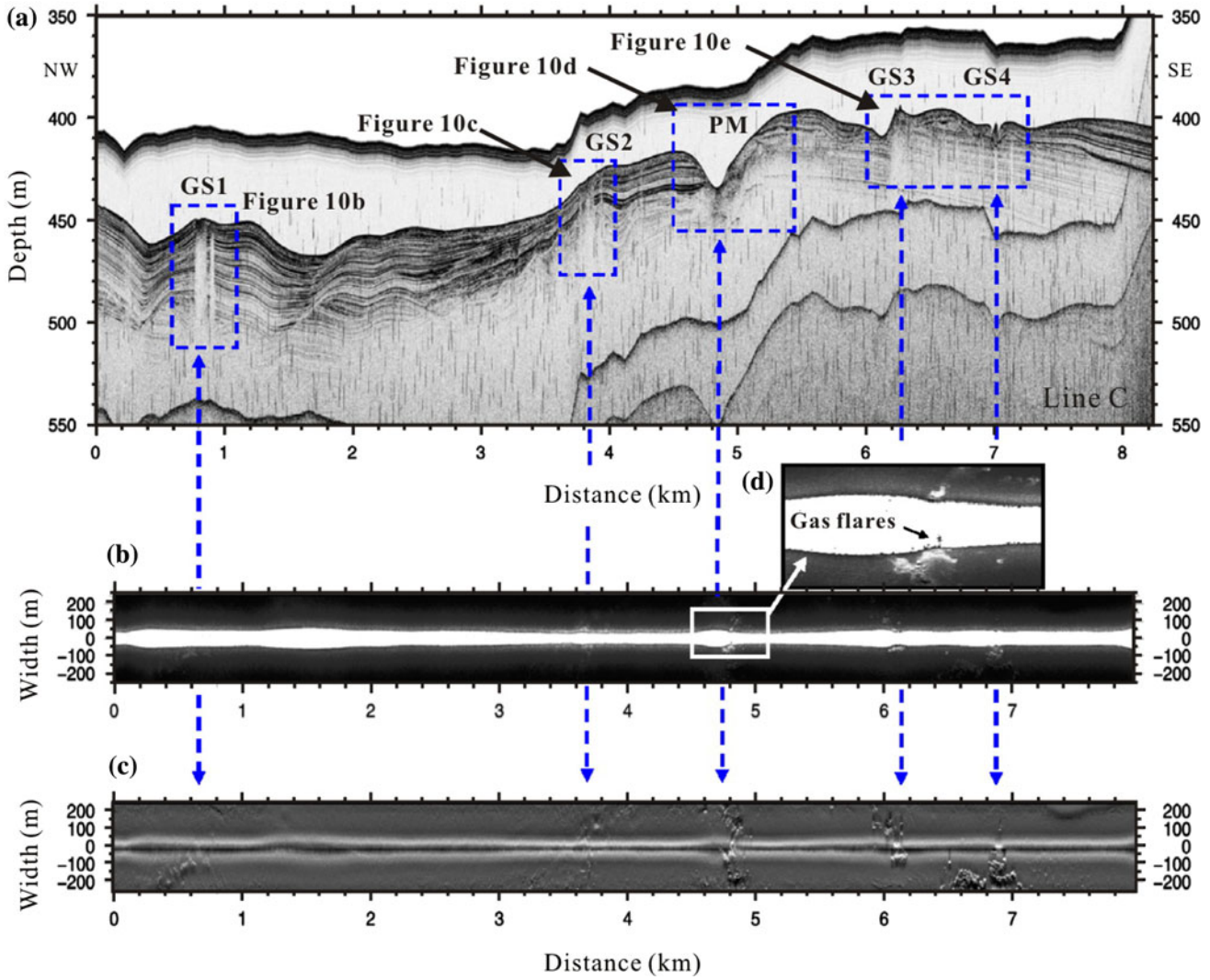

Fig. 7 Sub-bottom profiler and sidescan sonar images of *line C*. **a** Sub-bottom profiler image indicate four gas seeps (GS1, GS2, GS3 and GS4) and one pockmark (PM). The enlarged images are shown in Figs. 10b–e. **b** Sidescan sonar image without *bottom* lock. **c** Sidescan sonar image with *bottom* lock. *Note* that high backscatter intensity (*light tones*) exists at PM, GS3 and GS4 areas and the medium backscatter intensity exists at gas seep GS1 and GS2 areas. **d** Possible small gas flares. See the profile location in Fig. 2

seeps may also be covered by authigenic carbonates because relatively high backscatter intensity and rough seafloor characteristics are observed in the sidescan sonar image (Figs. 7 and 10e). The widths of GS3 and GS4 are about 175 and 135 m, respectively (Fig. 10e; Table 1). Because the locations of the gas seeps are all close to the anticline, we infer the source of the fluid has the same origin as the GS2 and PM areas (Fig. 5). The fluid conduits in terms of gas chimney are obvious below the gas seeps for the depth greater than 40 m (Fig. 10e). However, the top $\sim$8 m thick sedimentary layer has been uplifted; we suggest that the phenomenon is because of an overpressure of fluid charging beneath the uplifted layer (Fig. 10e). No gas emission is detected in the area between two gas seeps suggesting that the gas is trapped by the top sealing sedimentary layers.

Pockmark

For the first time, a pockmark structure is imaged off SW Taiwan. The pockmark PM is shown in the sub-bottom profiler line C (Figs. 5, 7 and 10d). The pockmark is located at the thick sedimentary strata, interbedding of muddy and sandy sediments. However, the acoustic signal is transparent beneath the pockmark. This seismic blanking phenomenon could be due to the existence of gas in the pathway. Some strong reflectors (Fig. 10d) could be ascribed to the presence of gas hydrates or authigenic carbonates (e.g. Sahling et al. 2008). Because of a shallow water depth, it is theoretically impossible for gas hydrates to exist in this area. Therefore, the strong reflectors could be caused by authigenic carbonates. The high backscatter intensity in the sidescan sonar image in the pockmark PM

Table 1 Locations and characteristics of the anticline, gas seeps, pockmark and mud volcanoes in the upper slope area off SW Taiwan between Kaoping and Fangliao canyons

Type	Coordinates latitude(N) longitude(E)	Size	Remark
Anticline	–	–	Identified from MCS data and displayed in NNE-SSW direction. The anticline structure diminishes landward and does not extend onshore
Pockmark (PM)	N: 22°10′12″ E: 120°24′15″	The ellipse-like pockmark is 600 m wide, 1,200 m long and a depression of 35 m at the center	Identified from sub-bottom profiler data. Several water column gas flares are observed in the sidescan sonar image and gas plume reach 100 m high above seafloor is found in the EK500 sonar image. The high backscatter intensity of sidescan sonar data is related to the authigenic carbonates formation on the seafloor and confirmed by seafloor photos
Gas seep (G96)	N: 22°11′03″ E: 120°24′38″	About 310 m wide and 5 m deep at the central part	Identified from sub-bottom profiler data. The gas plume reach 150 m high above seafloor is found in the EK500 sonar image. The medium backscatter intensity of sidescan sonar data is related to the bacteria mats formation on the seafloor and confirmed by seafloor photos
Gas seep (GS1)	N: 22°11′32″ E: 120°22′09″	About 190 m wide	Identified from sub-bottom profiler data. The gas plum reach 20 m high above seafloor is found in the EK500 sonar image
Gas seep (GS2)	N: 22°10′32″ E: 120°23′44″	About 175 m wide	Identified from sub-bottom profiler data
Gas seep (GS3)	N: 22°09′48″ E: 120°24′54″	About 175 m wide	Identified from sub-bottom profiler data
Gas seep (GS4)	N: 22°09′33″ E: 120°25′15″	About 135 m wide	Identified from sub-bottom profiler data
Mud volcano (MV1)	N: 22°09′31″ E: 120°23′18″	Diameter is about 1,500 and 100 m high	Identified from multibeam bathymetry
Mud volcano (MV2)	N: 22°08′30″ E: 120°22′23″	About 880 m long and 75 m high	Identified from multibeam bathymetry

area (Figs. 7 and 10d) is related to the authigenic carbonates as attested by seafloor photos of TowCam system (Fig. 8). As shown in the multibeam bathymetry, the ellipse-like pockmark is 600 m wide, 1,200 m long and a depression of 35 m at the center of the pockmark (Figs. 9 and 10d; Table 1). The MCS profiles show the deeper part of the pockmark also belongs to the anticline structure in Fig. 5. Several water column gas flares are observed in

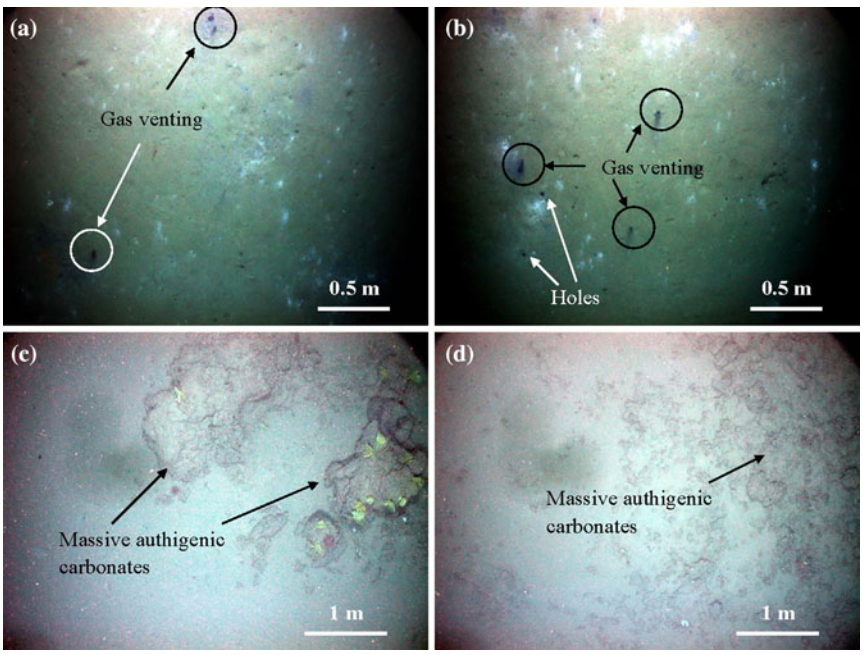

Fig. 8 Seafloor photos taken by deep-towed camera (TowCam) system. **a** and **b** are the photos taken at the gas seep G96 area, showing the bacteria mats in white patches and obvious gas venting activity. **c** and **d** are the photos taken at the pockmark PM area, showing the massive authigenic carbonates

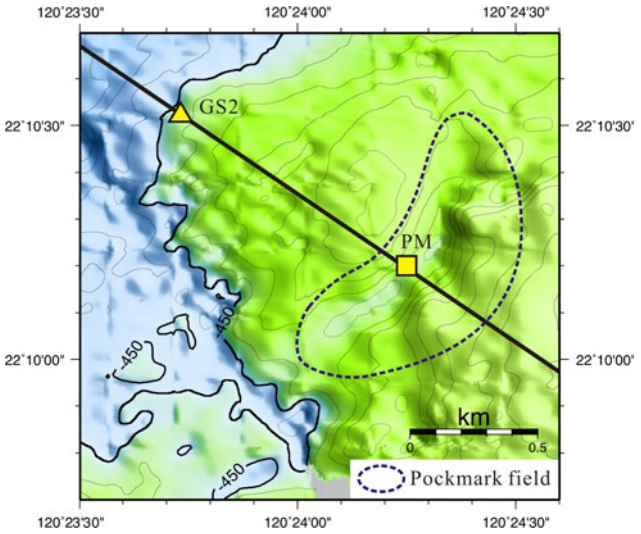

Fig. 9 The bathymetric map shows the possible pockmark PM area. The ellipse-like pockmark is about 600 m wide, 1,200 m long and a depression of 35 m at the center. The pockmark field is in NNE-SSW direction, roughly parallel to the anticline structure in Fig. 2

the sidescan sonar images (Fig. 7). A 100-m high gas plume in water column is also found in the EK500 sonar image (Fig. 5). The pockmark field is oriented NNE-SSW (Fig. 9), roughly parallel to the anticline structure (Fig. 12). We suggest that the occurrence of the pockmark is similar to that of the gas seep G96 though the surface of pockmark is covered by authigenic carbonates instead of the bacteria mats in the gas seep G96. Gas venting is found at the eastern flank but not at the center of the pockmark. It could be explained as a self-sealing nature of seeps because the carbonate cementation has gradually clogged the fluid migration pathways at the center (Hovland 2002).

Mud volcanoes

Based on the multibeam bathymetry, two mud volcanoes MV1 and MV2 are found in the south of the survey area (Figs. 2 and 11). Located at a water depth of about 465–365 m, the cone-shaped MV1 has a diameter of about 1,500 m and a height of 100 m (Fig. 11, Table 1). The MV2 is of about 880 m long and 75 m high, roughly elongated and parallel to the trend of the anticline structure (Figs. 2 and 11). Because a mud diapir structure below the two mud volcanoes was documented (Figs. 2 and 12) (Chuang 2006a; Sun and Liu 1993 and Lin et al. 2009), it could be typical that mud volcanoes overlie a diapir (Kopf 2002). The fluid coming from the mud diapir migrates through the fractures to seafloor. However, a detailed investigation for these two mud volcanoes is still necessary.

Discussion

Active gas venting and high methane flux

Several water column gas flares are observed in the sidescan sonar images along lines A and C. The EK500 sonar images also reveal three gas plumes in the sea water, above the gas seeps G96 and GS1 and pockmark PM areas. Moreover, the gas plumes associated with the gas seep G96 and pockmark PM are exactly located above the anticlinal ridge. In the east of the gas seep G96, a vertically faulted zone (Fig. 6) cutting through the shallow sedimentary layers provides an effective pathway for upward migration of the fluid. As mentioned previously, the upper ~8 m thick sedimentary stratum uplifted between the gas seeps GS3 and GS4 could be due to continuous fluid charging (Fig. 10e). It suggests that the fluid venting is very active and an existence of high pressure fluid in this area. In that case, the break up of the uppermost sedimentary stratum at GS4 could be due to the overpressure (Fig. 10e).

More than 25 piston and gravity cores collected from the upper slope area between Kaoping and Fangliao canyons at water depths between 300 and 1,000 m (Chuang et al. 2006). The results of a very high methane concentration and shallow sulfate/methane interface in some sediments indicate a relatively high methane flux below the seafloor (Chuang et al. 2006). These characteristics confirm the common occurrences of active fluids/gases vents in the area.

Fluid migration

According to the interpretation of MCS profiles, the anticline structure is related to the gas venting. The fluid may come from the deeper part of the anticline along faults or fractures and migrates upward to the seafloor. The analysis of stable carbon isotopes in sediments pore space at gas seep G96 area indicates that the gas is of thermogenic origin (Chuang 2006b). The thermogenic gas is also found at the station 15 (Oung et al. 2006), located in the west of Kaoping canyon (Fig. 1). Oung et al. (2006) suggested the thermogenic gas is associated with the faults acting as an efficient migration pathway for the vertical migration of thermogenic gas. Similarly, we suggest that existing faults at the deeper part of the anticline may be an efficient conduit for thermogenic gas to migrate upward to the seafloor.

Gas seep self-sealing

Hovland (2002) proposed that gas seeps generally undergo three stages of self-sealing process. The first stage includes the development of bacterial mats at sub-surface. The

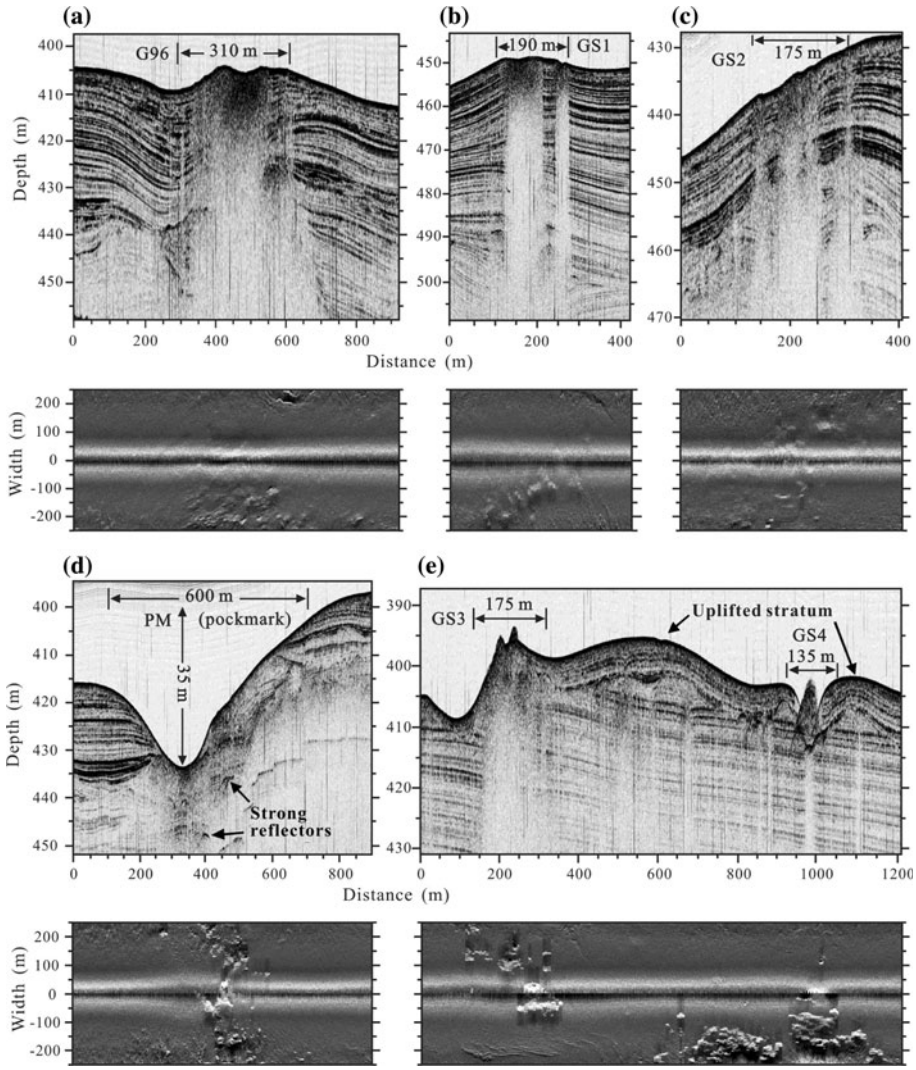

Fig. 10 *Sub-bottom* profiler and sidescan sonar images of gas venting features. *Sub-bottom* profiler image above and corresponding sidescan sonar image below. **a**, **b** and **c** of the gas seep G96, GS1 and GS2 areas represent medium backscatter intensity (*light tones*) and medium rough seafloor in sidescan sonar images. **d** and **e** of the pockmark PM and gas seep GS3 and GS4 areas represent high backscatter intensity (*light tones*) and high rough seafloor in sidescan sonar images

seepage rate is reduced in this stage. The second stage occurs when conduits have been filled up with sediments and bacterial mats are visible on the surface. Only intermittent ebullition occurs then. The final stage includes the development of carbonate cover over the seep area. No visible ebullition occurs at this stage. Based on the seafloor photos taken by TowCam system, the bacteria mats and massive authigenic carbonates exist on the seafloor (Fig. 8), which cause the relatively medium backscatter intensity at the gas seep G96 area and high backscatter intensity at the pockmark PM area of the sidescan sonar images. In addition, the massive authigenic carbonates and bacteria mats have also caused high rough seafloor at the pockmark PM area and medium rough seafloor at the gas seep G96 area.

The gas seep G96 is characterized by bacteria mats formation on the seafloor (Fig. 8) and active gas venting activity (Figs. 4 and 8). The pockmark PM seafloor is covered by massive authigenic carbonates (Fig. 8) and ongoing gas seep activity (Figs. 5 and 7). Therefore, we infer that the gas seep G96 area may be in a transitional stage from the first to second stage of the self-sealing process of the natural gas because the gas venting is still active (gas plume is observed). The pockmark PM area may be in a transitional stage from the second to final stage because of the ongoing gas seep activity (gas flares and gas plume are observed). It indicates that the occurrence of the gas seep activity in the pockmark PM area is older than that of the gas seep G96 area.

In the pockmark PM area, the gas plume is observed at eastern flank but not at bottom and authigenic carbonates exist below the bottom of the pockmark, which are identified based on sub-bottom profiler data as strong reflectors (Fig. 10d). According to the results, we suggest that the fluid migration pathways could have been clogged by carbonates at the bottom due to the process of gas seep self-sealing (Hovland 2002). The current fluid migration pathways thus have shifted to the eastern flank of pockmark.

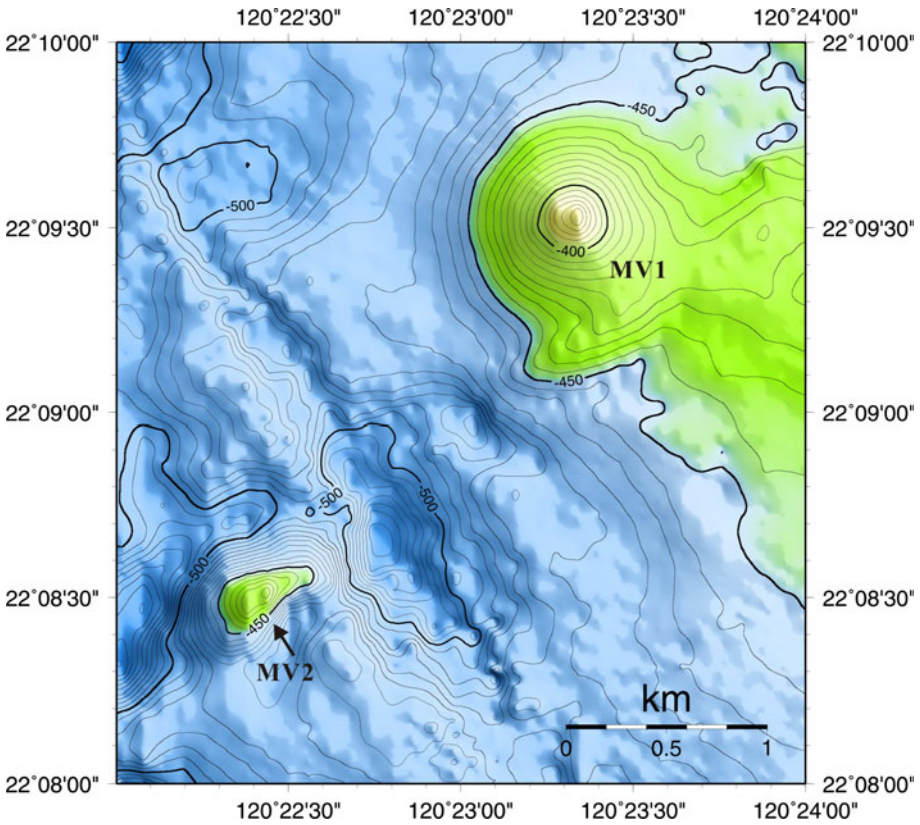

Fig. 11 The bathymetric map of two possible mud volcanoes MV1 and MV2. The MV2 is roughly elongated and parallel to the trend of the anticline in Fig. 2

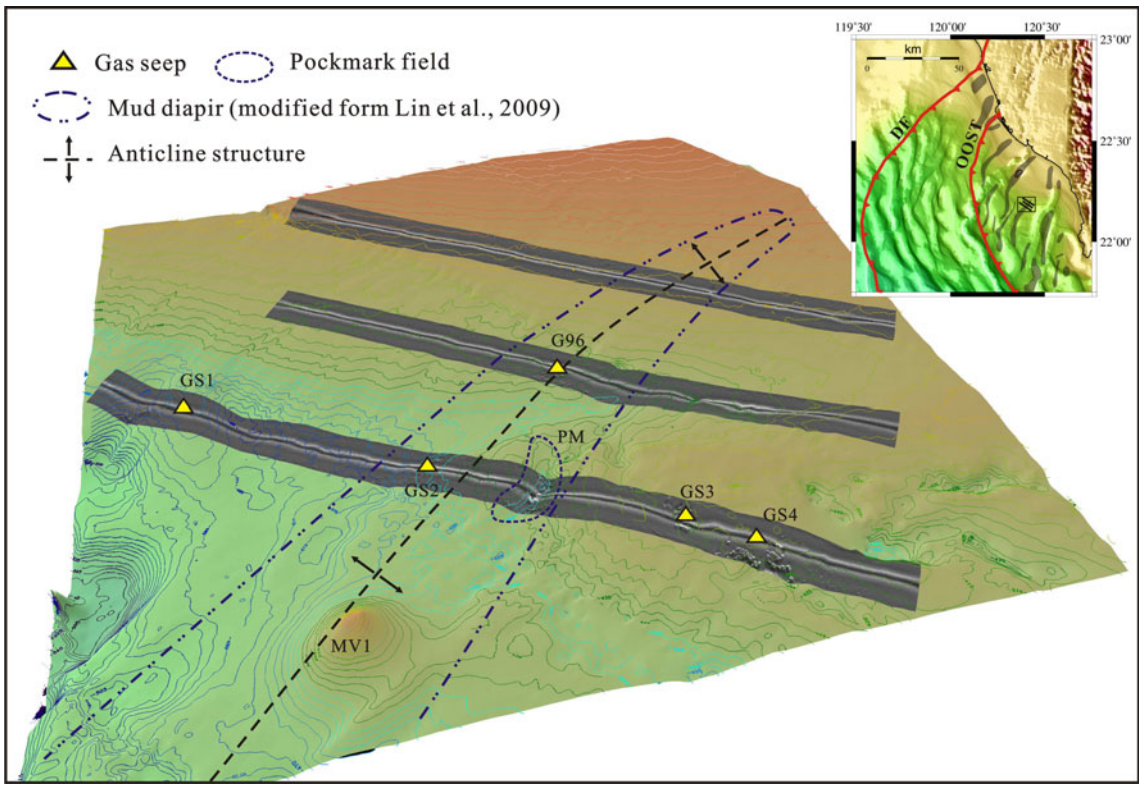

Fig. 12 Mosaic of deep-towed sidescan sonar images and the distribution map of gas venting features. The location of the study area is shown in the *upper right* inlet

Conclusions

1. The analysis of the deep-towed sidescan sonar and sub-bottom profiler data, collected in the near shore area off SW Taiwan between Kaoping and Fangliao canyons, has revealed five gas seeps (G96, GS1, GS2, GS3 and GS4) and one pockmark (PM).
2. The seafloor photos taken by TowCam system have shown that the relatively medium backscatter intensity of sidescan sonar image at the gas seep G96 and high backscatter intensity at the pockmark PM area are associated with the bacteria mats and authigenic carbonates formation on the seafloor due to the process of AMO, respectively.
3. Water column gas flares are observed in sidescan sonar images, especially above the line A and over pockmark PM areas. EK500 sonar images also show the gas plumes in the water column above the gas seep G96, pockmark PM and gas seep GS1 areas; the gas plumes reach as high as 150 m, indicating a very active gas venting in the near shore area off SW Taiwan.
4. The MCS profiles show that the anticline structure is closely related to the fluid migration. The fluid migrates from the anticline structure to its ridge summit, then to the seafloor through the fractures. The seafloor and seawater venting features are hence formed.
5. According to seafloor characteristic of gas seeps, the gas seep G96 area may be in a transitional stage from the first to second stage of the process of gas seep self-sealing. The pockmark PM area may be in a transitional stage from the second to final stage. It indicates that the occurrence of the gas seep activity in the pockmark PM area is older than that of the gas seep G96 area.
6. In the pockmark PM area, the fluid migration pathways could have been clogged by carbonates at the bottom due to the gas seep self-sealing process and the current pathway has shifted to the eastern flank of pockmark.

Acknowledgments We would like to thank the crew and the technical staff of the R/V Ocean Research I collecting the deep-towed sidescan sonar and seismic data used in this study. We thank Prof. S. Lin for conducting a deep-towed camera (TowCam) survey to collect seafloor photos used in this study. We also thank two anonymous reviewers for their comments and suggestions that improved much the manuscript. This study is mainly supported by Central Geological Survey, Ministry of Economic Affairs, Taiwan, under grants 96-5226903000-01-01.

References

Blondel P, Murton BJ (1997) Handbook of seafloor sonar imagery. Wiley–Praxis Series in Remote Sensing, John Wiley and Sons Ltd. in association with Praxis Publishing Ltd, Chichester, p 314

Brown KM (1990) The nature and hydrogeologic significance of mud diapirs and diatremes for accretionary systems. J Geophys Res 95(B6):8969–8982

Bünz S, Mienert J (2004) Acoustic imaging of gas hydrate and free gas at the Storegga Slide. J Geophys Res 109:B04102. doi: 10.1029/2003JB002863

Bünz S, Mienert J, Berndt C (2003) Geological controls on the Storegga gas-hydrate system of the mid-Norwegian continental margin. Earth Planet Sci Lett 209:291–307

Chiu JK, Liu CS (2008) Comparison of sedimentary process on adjacent passive and active continental margins offshore of SW Taiwan. Basin Res 20:503–518

Chiu JK, Tseng WH, Liu CS (2006) Distribution of gassy sediments and mud volcanoes offshore southwestern Taiwan. Terr Atmos Ocean Sci 17:703–722

Chuang HJ (2006a) Distribution and structural relationships of mud diapirs offshore southwestern Taiwan, Thesis. Inst Oceanogr Natl. Taiwan Univ., Taiwan, 113 pp (in Chinese)

Chuang PC (2006b) Gas geochemistry study in gas hydrate potential areas offshore SW Taiwan, Thesis. Inst Geol Sci Natl. Taiwan Univ., Taiwan, 83 pp (in Chinese)

Chuang PC, Yang TF, Lin S, Lee HF, Lan TF, Hong WL, Liu CS, Chen JC, Wang Y (2006) Extremely high methane concentration in bottom water and cored sediments from offshore southwestern Taiwan. Terr Atmos Ocean Sci 17:903–920

Deyhle A, Kopf A (2001) Deep fluids and ancient pore waters at the backstop: stable isotope systematics (B, C, O) of mud volcano deposits on the Mediterranean Ridge accretionary wedge. Geology 29(11):1031–1034

Dimitrov LI (2002) Mud volcanoes-the most important pathway for degassing deeply buried sediments. Earth-Sci Rev 59:49–76

Dimitrov LI (2003) Mud volcanoes—a significant source of atmospheric methane. Geo-Mar Lett 23:155–161

Holland CW, Weber TC, Etiope G (2006) Acoustic scattering from mud volcanoes and carbonate mounds. J Acoust Soc Am 120:3553–3565

Hovland M (2002) On the self-sealing nature of marine seeps. Conti Shelf Res 22:2387–2394

Hovland M, Curzi PV (1989) Gas seepage and assumed mud diapirism in the Italian central Adriatic Sea. Mar Petrol Geol 6:161–169

Iacono CL, Gràcia E, Diez S, Bozzano G, Moreno X, Dañobeitia J, Alonso B (2008) Seafloor characterization and backscatter variability of the Almería Margin (Alboran Sea, SW Mediterranean) based on high-resolution acoustic data. Marine Geol 250:1–18

Jiang WT, Chen JC, Huang BJ, Chen CJ, Lee YT, Huang PR, Lung CC, Huang SW (2006) Mineralogy and physical properties of cored sediments from the gas hydrate potential area of offshore southwestern Taiwan. Terr Atmos Ocean Sci 17:981–1007

Johnson JE, Goldfinger C, Suess E (2003) Geophysical constraints on the surface distribution of authigenic carbonates across the Hydrate Ridge region, Cascadia margin. Marine Geol 202: 79–120

Klaucke I, Sahling H, Weinrebe W, Blinova V, Bürk D, Lursmanashvili N, Bohrmann G (2006) Acoustic investigation of cold seeps offshore Georgia, eastern Black Sea. Marine Geol 231:51–67

Kopf AJ (2002) Significance of mud volcanism. Rev Geophys 40(2):1–52

Krastel S, Spiess V, Ivanov M, Weinrebe W (2003) Acoustic investigations of mud volcanoes in the Sorokin Trough, Black Sea. Geo-Mar Lett 23:230–238

Lin S, Hsieh WC, Lim YC, Yang TF, Liu CS, Wang Y (2006) Methane migration and its influence on sulfate reduction in the

Good Weather Ridge region, South China Sea continental margin sediments. Terr Atmos Ocean Sci 17:883–902

Lin AT, Liu CS, Lin CC, Schnürle P, Chen GY, Liao WZ, Teng LS, Chuang HJ, Wu MS (2008) Tectonic features associated with the overriding of an accretionary wedge on top of a rifted continental margin: an example from Taiwan. Marine Geol 255:186–203

Lin AT, Yao B, Hsu SK, Liu CS, Huang CY (2009) Tectonic features of the incipient arc-continent collision zone of Taiwan: Implications for seismicity. Teconophysics 479:28–42

Liu CS, Huang IL, Teng LS (1997) Structure features off southwestern Taiwan. Marine Geol 137:305–319

Liu CS, Deffontaines B, Lu CY, Lallemand S (2004) Deformation patterns of an accretionary wedge in the transition zone from subduction to collision offshore southwestern Taiwan. Mar Geophys Res 25:123–137

Liu CS, Schnürle P, Wang Y, Chung SH, Chen SC, Hsiuan TH (2006) Distribution and characters of gas hydrate offshore of southwestern Taiwan. Terr Atmos Ocean Sci 17:615–644

Mienert J, Vanneste M, Bünz S, Andreassen K, Haflidason H, Sejrup HP (2005) Ocean warming and gas hydrate stability on the mid-Norwegian margin at the Storegga Slide. Mar Petrol Geol 22:233–244

Milkov AV (2000) Worldwide distribution of submarine mud volcanoes and associated gas hydrates. Marine Geol 167:29–42

Naudts L, Greinert J, Artemov Y, Staelens P, Poort J, Van Rensbergen P, De Batist M (2006) Geological and morphological setting of 2778 methane seeps in the Dnepr paleo-delta, northwestern Black Sea. Marine Geol 227:177–199

Naudts L, Greinert J, Artemov Y, Beaubien SE, Borowski C, De Batist M (2008) Anomalous sea-floor backscatter patterns in methane venting areas, Dnepr paleo-delta, NW Black Sea. Marine Geol 251:253–267

Orange DL, Yun J, Maher N, Barry J, Greene G (2002) Tracking California seafloor seeps with bathymetry, backscatter and ROVs. Cont Shelf Res 22:2273–2290

Oung JN, Lee CY, Lee CS, Kuo CL (2006) Geochemical study on hydrocarbon gases in seafloor sediments, southwestern offshore Taiwan—implications in the potential occurrence of gas hydrates. Terr Atmos Ocean Sci 17:921–931

Reed DL, Lundberg N, Liu CS, Kuo BY (1992) Structural relations along the margins of the offshore Taiwan accretionary wedge: implications for accretion and crustal kinematics. Acta Geol Taiwan 30:105–122

Sahling H, Bohrmann G, Spiess V, Bialas J, Breitzke M, Ivanov M, Kasten S, Krastel S, Schneider R (2008) Pockmarks in the Northern Congo Fan area, SW Africa: Complex seafloor features shaped by fluid flow. Marine Geol 249:206–225

Sun SC, Liu CS (1993) Mud diapir and submarine channel deposits in offshore Kaosiung-Hengchun, southwest Taiwan. Petro Geol Taiwan 28:1–14

Talukder AR, Bialas J, Klaeschen D, Buerk D, Brueckmann W, Reston T, Breitzke M (2007) High-resolution, deep tow, multichannel seismic and sidescan sonar survey of the submarine mounds and associated BSR off Nicaragua pacific margin. Marine Geol 241:33–43

Tréhu AM et al (2003) Proceedings of the ocean drilling program, initial report, vol 204, Ocean Drill. Program, College Station, Tex

Wang Y, Liu CS, Chen JC, Chung SH, Lin S, Chen SC, Chen PC (2007) Gas hydrate investigation in Taiwan: recent progress and future development. In: Proceedings of the international conference on gas hydrate-energy, climate and environment, October, 4–5, 2007, Taiwan, pp 21–25

Yang TF, Yeh GH, Fu CC, Wang CC, Lan TF, Lee HF, Chen CH, Walia V, Sung QC (2004) Composition and exhalation flux of gases from mud volcanoes in Taiwan. Environ Geol 46: 1003–1011

Yang TF, Chuang PC, Lin S, Chen JC, Wang Y, Chung SH (2006) Methane venting in gas hydrate potential area offshore of SW Taiwan: evidence of gas analysis of water column samples. Terr Atmos Ocean Sci 17:933–950